Multiple Transonic Shock-Wave/Turbulent Boundary-Layer Interaction in a Circular Duct

Deepak Om* and Morris E. Childs†
University of Washington, Seattle, Washington

An experimental study is described in which detailed pitot, static, and wall pressure measurements have been obtained for multiple transonic shock-wave/turbulent boundary-layer interactions in a circular duct at a freestream Mach number of 1.49, a unit Reynolds number of 4.90×10^6/m, and a blockage of 5.15%. The details of the flowfield show the formation of a series of normal shock waves with successively decreasing strength and decreasing distance between the successive shock waves up to the point where a terminal shock occurs. A one-dimensional flow model based on the boundary-layer displacement thickness is postulated to explain the formation of the series of normal shock waves. A comparison with the results from our previous study involving a single shock interaction suggests that the effect of increased blockage is to promote multiple shock interactions and produce a lower pressure recovery, a less retarded boundary-layer flow, and an increase in the overall length of the interaction.

Nomenclature

A = area of the duct
B = blockage, $A_{\delta_u^*}/A = [1-(1-\delta_u^*/R)^2]$
c_f = skin-friction coefficient, $=2\tau_w/\rho_e u_e^2$
D = diameter of the duct
H = shape factor, $=\delta^*/\theta$
M = Mach number
P = pressure
R = radius of the duct
Re = Reynolds number
u = streamwise velocity
x = axial distance
$\bar{X}$ = $(x-x_u)/D$
$\bar{X}$ = $(x-x_u)/\delta_u$
y = radial distance from the wall
$\bar{Y}$ = y/δ_u
δ = boundary-layer thickness
δ^* = displacement thickness, given by

$$\delta^*-\frac{\delta^{*2}}{2R}=\int_0^{\delta}\left(1-\frac{\rho u}{\rho_e u_e}\right)\left(1-\frac{y}{R}\right)\mathrm{d}y$$

θ = momentum thickness, given by

$$\theta-\frac{\theta^2}{2R}=\int_0^{\delta}\frac{\rho u}{\rho_e u_e}\left(1-\frac{u}{u_e}\right)\left(1-\frac{y}{R}\right)\mathrm{d}y$$

ρ = density
τ = shear stress

Subscripts

e = boundary-layer edge
u = start of interaction
w = wall value
0 = stagnation condition
∞ = freestream condition at the start of interaction

Presented as Paper 83-1744 at the AIAA 16th Fluid and Plasma Dynamics Conference, Danvers, Mass., July 12-14, 1983; received July 2, 1984; revision received Oct. 30, 1984.

*Research Assistant Professor, Department of Mechanical Engineering; currently with Boeing Commerical Airplane Company, Seattle, WA. Member AIAA.

†Professor, Department of Mechanical Engineering. Member AIAA.

Introduction

THE structure of shock-wave/boundary-layer interactions in a confined duct has important implications in the design and operation of wind tunnel diffusers[1] and in inlets of airbreathing engines.[2] Studies of such interactions are also important for diffuser applications in gas dynamic lasers,[3] where relatively thick boundary layers may be present in narrow channels. Another application is in the design of high-speed centrifugal compressors, where the speed at the impeller tip is often supersonic. The pipe diffuser used with such a compressor has resulted in significant improvements in stage efficiency operating in transonic approach flow.[4]

There have been numerous investigations[5-9] in which the influence of parameters such as Mach number, Reynolds number, diameter of pipe, and upstream boundary-layer thickness on pressure recovery has been studied for shock-wave/turbulent boundary-layer interactions in confined ducts. Lustwerk[5] tested a sharp-lipped duct in a wind tunnel with a freestream Mach number of 2.05. He found that with no upstream boundary layer, a plane normal shock wave was formed. As the boundary layer thickened, a series of plane or lambda shock waves occurred and, with further thickening, a series of oblique shock waves was formed. Merkli[7] studied the influence of the Reynolds number, Mach number, upstream displacement thickness, and duct length on the pressure recovery in a rectangular constant-area supersonic duct. Kamal and Livesey[8] studied the dependence of diffuser inlet conditions on the preceding shock-wave/boundary-layer interaction variables; namely, the length of the parallel circular pipe, the position of the shock wave within the inlet pipe, and the tunnel stagnation pressure level. However, neither Merkli nor Kamal and Livesey studied the details of the shock structure. Waltrup et al.[6,9] measured in-stream pitot pressure and wall shear at a freestream Mach number of 2.60 and at a Reynolds number based on upstream momentum thickness of 2.67×10^4 and showed that the multiple shock structure in their cylindrical duct was oblique and separated. They also studied the influence of Mach number, Reynolds number based on upstream momentum thickness, duct diameter, and the upstream momentum thickness on pressure recovery. In all of the above investigations, however, data on the boundary-layer flow are almost nonexistent.

The study described herein is a continuation of the work reported in Ref. 10 where the results of studies of single

shock interactions in a circular duct were presented. The present paper describes the mean-flow results obtained for multiple shock interactions in a circular duct. The experiment was performed at a freestream Mach number of 1.49, a Reynolds number based on upstream momentum thickness of 1.95×10^3, and a blockage of 5.15%. An axisymmetric experimental configuration was chosen to minimize the three-dimensional effects known to be present for shock-wave/boundary-layer interactions in rectangular channels.[11-13]

Experiment

The experiment was performed in the continuous-flow facility[14] at the University of Washington. The facility is shown schematically in Fig. 1. An axisymmetric nozzle designed for a Mach number of 1.6 was used in conjunction with a 51.9-mm-diam test section. The contour of the nozzle was not corrected for boundary-layer growth. The overall length of the plexiglas nozzle test section facility was 44.45 cm. Wall static pressure taps were located on a line in the test section at intervals of 5.1 mm. Additional taps were located at 90-deg intervals around the test section from this primary line to check the flow symmetry. A single row of rectangular boundary-layer trips was cemented to the nozzle wall 25.4 mm upstream of the throat to make sure the test section boundary layer was turbulent. The trips, made of 150-grit sandpaper, were 0.33 mm thick and 2.54 mm wide.

The multiple shock system was positioned in the test section by using a blunt cone as a centerbody to choke the flow at the exit from the test section. In Ref. 10, it was shown that a single normal shock wave was generated in the test section at nearly the same freestream Mach number and unit Reynolds number when blockage, B $(=A_{\delta_u^*}/A)$, was equal to 2.27%; where blockage is defined as the effective area reduction due to boundary layer at the upstream location, divided by the duct area.

A 55.88-mm-long by 5.08-mm-wide slot cut through the diffuser wall near the upstream end was used for the longitudinal and radial translation of the probes. The probe slot was offset azimuthally from the primary line of wall static pressure ports. Pitot and static pressure probes with distances from the stem centerline to the measuring location of 101 and 197 mm were used to measure the pressures. Boundary-layer measurements with the longer probe were checked against measurements with the shorter probe to make sure that there was no deflection of the probe tip due to dynamic pressure at the operating total pressure. The 197-mm-long probe was used to obtain data throughout the interaction; however, the profiles at a few axial locations near the end of the interaction were obtained by means of the 101-mm probe. The 197-mm probe could be translated over the length of the measuring locations with the addition of extension sections between the test section and diffuser. The extension section had a constant diameter of 51.9 mm and a length of 47.6 mm. The flow in the test section was not affected by the addition of extension sections, as determined by checking the wall static pressure distribution.

The probes were inserted into the test section from the diffuser to minimize the blockage of the flow. Small changes in blockage due to traversing of the probe were offset by moving the centerbody and ensuring that the shock system remained in a fixed position in the test section. The wall pressure distribution was used to monitor the location of the shock system. A discussion of blockage effect due to the presence of the probe is given in Ref. 15.

Pitot pressures were measured with a flattened pitot tube, for which the probe tip was approximately 0.254 mm high and the opening approximately 0.10 mm high by 0.38 mm wide. Local static pressures were measured with a cone-cylinder probe of the type described in Ref. 16. The same probe was used to obtain the results reported in Ref. 10. The outer diameter of the probe was 1.06 mm. Two 0.16-mm-diam static pressure ports, located 10.6 mm downstream of the cone-cylinder junction, were drilled at ±40 deg circumferentially from the side of the probe that was closest to the test section wall. Static pressure ports at these locations make the probe relatively insensitive to flow inclination in the range of −2 to +6 deg. The probes and instrumentation are described in detail in Ref. 17.

Following Ref. 18, the experimental uncertainty of the measured pressures was estimated as $\pm(F+\sigma t_{95})$, where F is the fixed error, σ the standard deviation of a set of repeated measurements, and t_{95} the 95th precentile of the student-t distribution. The uncertainty was ±0.5% for wall pressure, ±1.0% for pitot pressure, ±0.5% and ±5.0% for static pressure.

The test facility was operated with dry air at a nominal freestream stagnation temperature of 300 K (±1%) with adiabatic wall conditions. The freestream Mach number was 1.49 and the unit Reynolds number based on the freestream static temperature was 4.90×10^6/m.

Table 1 Experimental flow conditions and upstream boundary-layer parameters for the multiple shock interactions

$P_0=0.3325$ atm	$\delta_u^*=1.001$ mm
$M_\infty=1.49$	$\theta_u=0.399$ mm
$Re/m=4.90\times10^6$	$C_{f_u}=0.002908$
$\delta_u=5.15$ mm	$B=0.0515$

Results and Discussion

The detailed experimental mean-flow structure for the multiple shock interactions is presented in this section. A summary of the experimental test conditions and upstream boundary-layer parameters used as normalization factors is given in Table 1. The distances $\bar{X}$ and $\tilde{X}$, as used in the text, are measured from the point of the initial wall pressure rise and are normalized by the boundary-layer thickness δ_u at the start of the wall pressure rise and the diameter of the duct D, respectively.

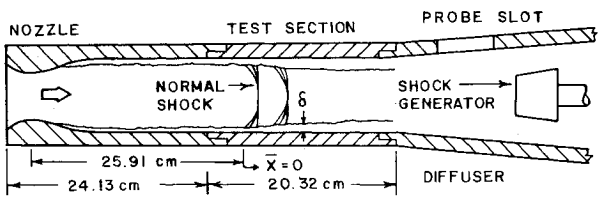

Fig. 1 Schematic of experimental facility.

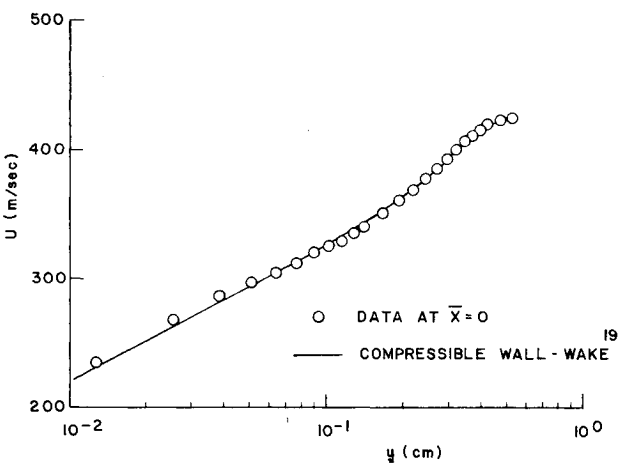

Fig. 2 Comparison of upstream experimental velocity profile with compressible wall-wake profile.

The upstream experimental boundary-layer profile is shown in semilogarithmic form in Fig. 2. Also shown for comparison is the compressible wall-wake profile,[19] with which the data points are in good agreement. The skin friction at the upstream location is within 8% of the zero pressure gradient flat-plate value as determined from Ref. 20. The upstream boundary layer is typical of a turbulent equilibrium boundary-layer profile.

Wall Pressure

In Fig. 3, wall pressure is normalized by the value just upstream of the initial pressure rise. The steepest slope in the wall pressure is observed at the start of the interaction. The overall pressure recovery amounts to about 75% of the ideal single normal shock pressure recovery at the same freestream Mach number. The Reynolds number based on the duct diameter Re_D, the freestream Mach number M_∞, and the blockage B, are recognized as the governing parameters for pressure recovery in supersonic diffusers.[7] A comparison with the wall pressure distribution of Ref. 10, as shown in Fig. 3, at nearly the same M_∞ and Re_D but at a lower blockage of 2.27%, suggests that the pressure recovery decreases with increasing blockage.

Static Pressure

Figure 4 shows the static pressure distributions. This figure has been derived from 38 radial static pressure profiles that can be found in Ref. 15. It shows strong pressure gradients in the radial direction that decrease in the streamwise direction. At $\bar{Y}=3.97$, the successive sudden increase in the static pressure is due to the presence of the successive normal shock waves. (The presence of the normal shock waves will be confirmed in the next subsection entitled "Mach Number" where it is shown that the flow becomes subsonic just downstream of each shock wave.)

In the region just ahead of a relatively strong normal shock wave and outside of the boundary layer, measured static pressures are known to be influenced by probe interference effects.[10,17] For this reason, the static pressure in the region just ahead of the first normal shock wave was determined by using the pitot pressure and tunnel stagnation pressure as the local total pressure (since losses through the emanating compression waves from the boundary layer are small). On the other hand, for weaker normal shock waves, e.g., for a single shock interaction at $M_\infty \simeq 1.3$,[17] the agreement between the measured static pressure and the static pressure determined from the pitot pressure was found to be within 6%. It is felt that for the present multiple shock interaction study, the measured static pressure should be fairly accurate in the region just upstream of the second and subsequent shock waves since these shock waves are much weaker in strength than the initial shock wave. (The reasons for the weaker strength will be discussed in the subsection entitled "Mach Number.") Probe interference effects on the measured static pressures just downstream of normal shock waves are typically very small. For a single shock interaction at $M_\infty = 1.48$, an axial survey of measured static pressure at $\bar{Y}=5.8$ indicated that the pressure just downstream of the normal shock wave had recovered to within 3% of the inviscid value.[17]

The static pressure peaks shown in Fig. 4 for $\bar{Y}=3.97$ are not necessarily the true peak values. More data points at finer intervals would be required to establish the true peaks. At $\bar{X}=15.79$, the flagged symbol represents measured static pressure for $\bar{Y}=3.67$. Measurements at this axial location were not obtained at higher values of $\bar{Y}$ because of the unsteadiness of the static pressure readings, perhaps due to the measuring port on the probe being too close to the shock wave.

Mach Number

Figure 5 shows Mach number contours for the flowfield. The contours were determined from pitot and static pressures except in the region ahead of the first shock wave and outside the boundary layer, where Mach number was determined using pitot and tunnel stagnation pressures. Because it was not possible to obtain schlieren or shadowgraph pictures of the flow in the circular duct, the exact structure and the location of the shock waves could not be determined. Approximate shock locations, as determined from radial static pressure profiles (which can be found in

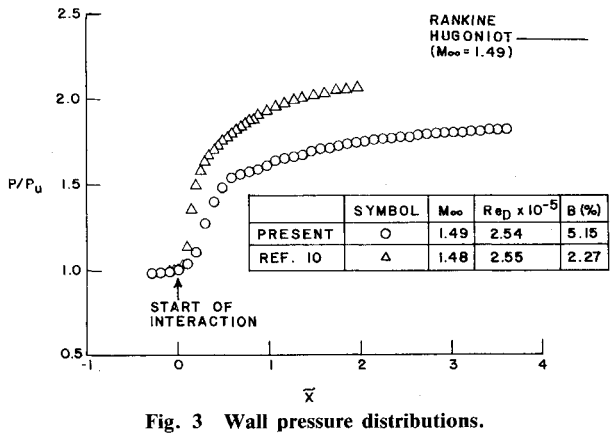

Fig. 3 Wall pressure distributions.

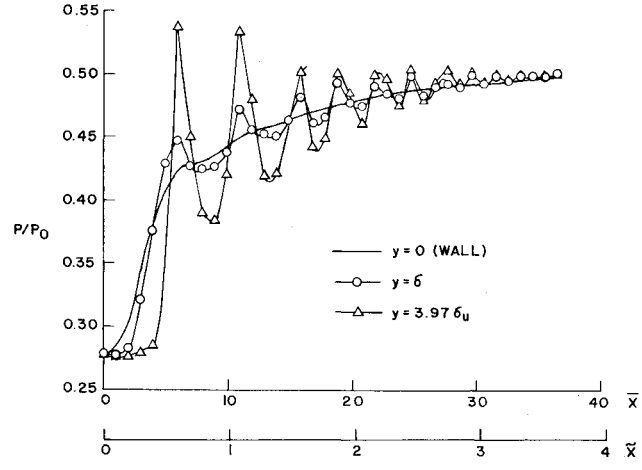

Fig. 4 Static pressure distributions.

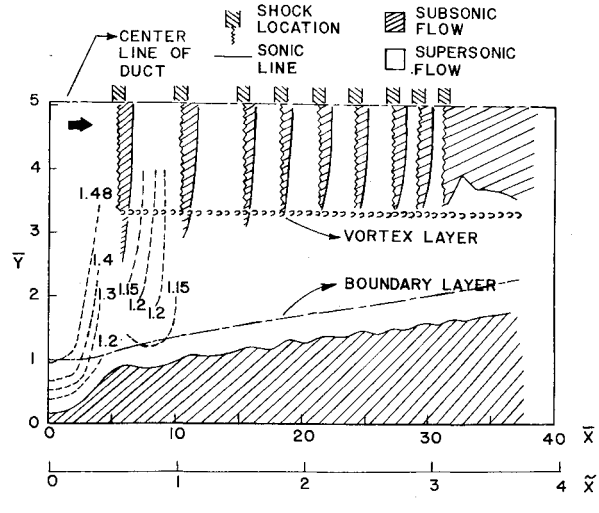

Fig. 5 Mach number contours.

Ref. 15), are indicated in Fig. 5. Measurements were not obtained beyond $\bar{Y}=3.97$; thus, the shock structure shown in Fig. 5 has been extrapolated up to the centerline of the duct. The approximate location of the vortex layer was determined from the pitot pressure profiles by noting the sudden change in pitot pressure. The pitot pressure profiles can be found in Ref. 15. The vortex layer originates from the first shock wave at about $\bar{Y}=3.3$. The formation of the vortex layer is similar to that in the case of a single normal shock interaction.[10,21] This vortex layer seems to persist through the complete interaction. No such vortex layer seemed to originate from subsequent shock waves, apparently because the shock waves are much weaker in strength.

The Mach number in the region just outside the boundary layer remains supersonic throughout the interaction, but, in the core region of the test section, the flow undergoes successive changes from supersonic to subsonic, which indicates the presence of the successive normal shock waves. The distance between the successive shock waves decreases. The flow remains mixed supersonic-subsonic at $\bar{X}=36.51$, although normal shock waves cease to exist in the core flow. Flowfield measurements were not obtained downstream of $\bar{X}=36.51$, but Fig. 5 seems to indicate that at successive downstream stations, the radial extent of the supersonic region will decrease until it terminates, thus forming an embedded supersonic region in an otherwise subsonic flow. This behavior is similar to the formation of large embedded supersonic regions for single shock interactions in confined ducts.[10]

At $\bar{Y}=3.97$, the Mach number just in front of the first shock wave was found to be 1.47. It was calculated using pitot pressure and the tunnel stagnation pressure as the local total pressure. This suggests that because of the coaxial nature of the flow, even at $\bar{Y}=3.97$ the compression waves emanating from the boundary layer are coalescing with the first normal shock wave. At $\bar{Y}=3.97$, just downstream of the first shock wave, the measured pitot pressure corresponds to the value that would be achieved through a shock angle of 83.5 deg at a Mach number of 1.47. This suggests that there may be some curvature of the shock wave in this region. The shock angle would increase for higher values of $\bar{Y}$ with the shock becoming purely normal at the centerline of the duct ($\bar{Y}=5.04$).

The Mach number distribution at $\bar{Y}=3.97$ is shown in Fig. 6. At $\bar{X}=15.79$, the flagged symbol represents the Mach number at $\bar{Y}=3.67$, because measurements were not obtained at higher values of $\bar{Y}$ due to the unsteadiness of the static pressure readings. Figure 6 indicates that the Mach number just ahead of the successive shock waves decreases, implying that the strength of each successive wave is weaker.

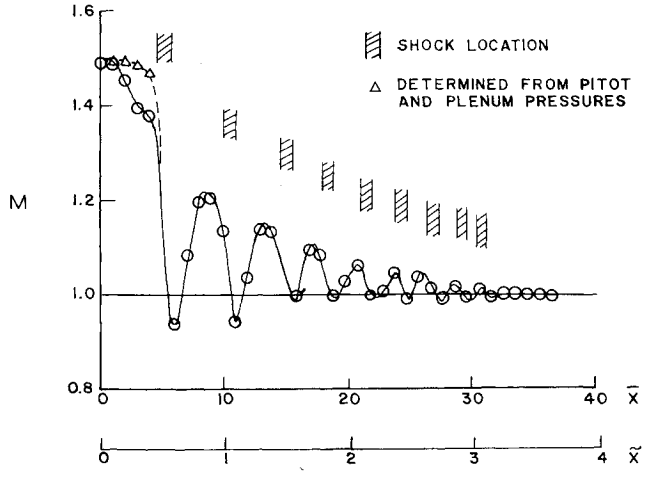

Fig. 6 Mach number distribution at $\bar{Y}=3.97$.

Skin Friction

The skin-friction distribution, as shown in Fig. 7, was determined from the experimental mean velocity profiles using the law-of-the-wall fit of Rubesin et al.[22] Details regarding the determination of the skin friction can be found in Refs. 17 and 22. Skin friction decreases rapidly and then increases as the flow passes through the first shock wave. After the first shock wave, the skin friction starts to increase and is affected only slightly as it goes through subsequent weaker shock waves. The skin-friction distribution indicates an unseparated interaction. The alcohol technique[14] did not show any separation of the flow as well. A comparison with the results of Ref. 10, as shown in Fig. 7, at nearly the same M_∞ and Re_D but at a lower blockage of 2.27%, indicates that the effect of increased blockage is to reduce the extent of separation or to eliminate it and produce a less retarded boundary-layer flow.

In Ref. 10, it was shown that the skin friction at $\bar{X}=1.98$ was 27.5% lower than the zero pressure gradient flat-plate value at the corresponding Mach and Reynolds numbers, as determined from Ref. 20. In the present experiment, skin friction at $\bar{X}=3.62$ is still 27.4% lower than the zero pressure gradient flat-plate value at the corresponding Mach and Reynolds numbers. A comparison of the present results with those of Ref. 10 indicates that the effect of increased blockage is to increase the overall length of the interaction.

Displacement and Momentum Thicknesses

The displacement thickness, as shown in Fig. 8, builds up rapidly across the first shock wave and then decreases slightly before it starts to increase due to the effect of the second shock wave. This process continues as the flow goes through the successive shock waves. An increased blockage (because of an increase in the upstream boundary-layer thickness) provides the means for the effective area modulation which is responsible for the formation of the multiple normal shock waves. Although the flow is far from one-dimensional, the formation of multiple normal shock waves can be explained through an equivalent one-dimensional flow model. The shock positions in the duct and the corresponding displacement buildup are shown, approximately, in Fig. 9. The displacement buildup due to the first shock wave is large enough to choke the flow. The subsonic flow, immediately behind the first shock wave, accelerates in the converging channel between sections AA and BB until the sonic throat BB is reached (Fig. 9). After section BB, supersonic expansion takes place and this supersonic region is terminated by the formation of the second normal shock wave. The displacement buildup due to the second normal shock wave chokes the flow again and the same process, as described for the first normal shock wave, takes place. The second normal

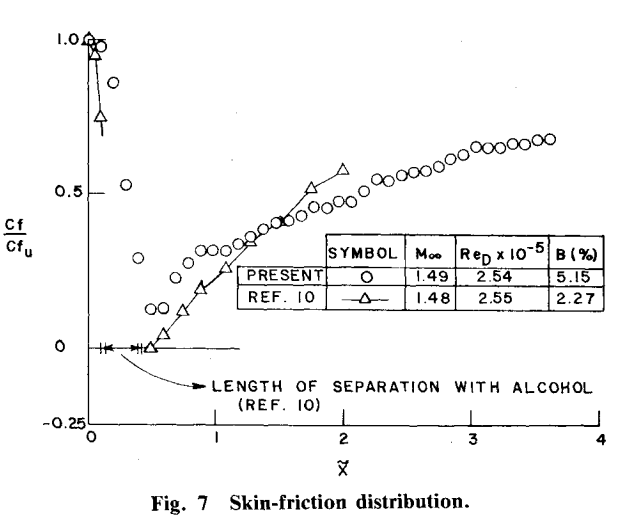

Fig. 7 Skin-friction distribution.

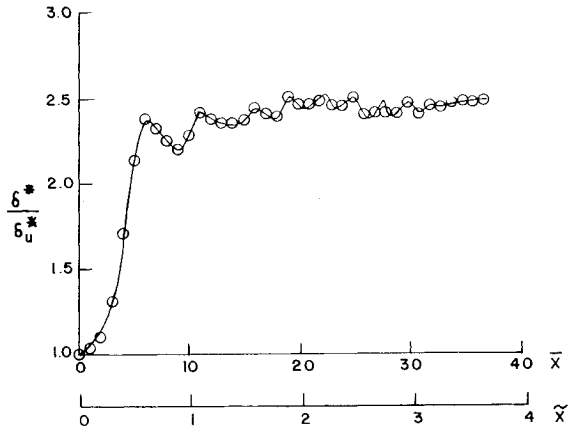

Fig. 8 Displacement thickness distribution.

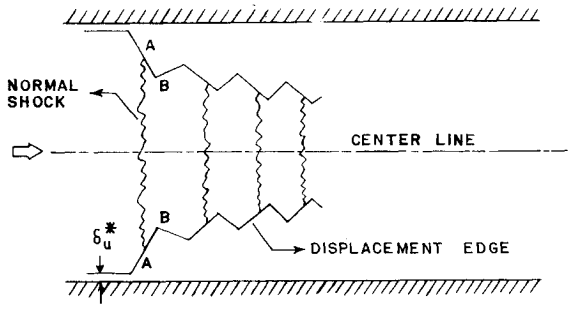

Fig. 9 One-dimensional flow model.

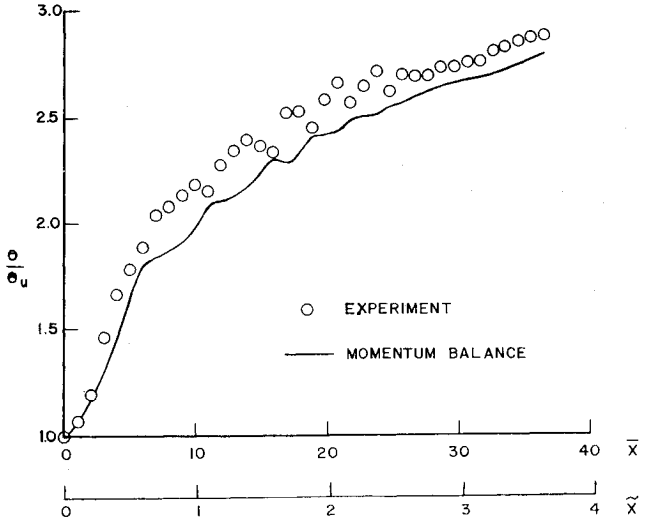

Fig. 10 Momentum thickness distribution.

shock wave, in turn, produces another normal shock wave. This process continues until the strength of the normal shock wave becomes weak enough that the flow does not become choked again.

The overall momentum thickness, shown in Fig. 10, increases in the downstream direction. The shape factor distribution (δ^*/θ) is shown in Fig. 11. The repeated pattern of a shape factor increase followed by a decrease indicates the presence of the multiple shock waves.

Two-Dimensionality of the Flow

An indirect check of the two-dimensionality of the flow was performed by substituting measured integral properties

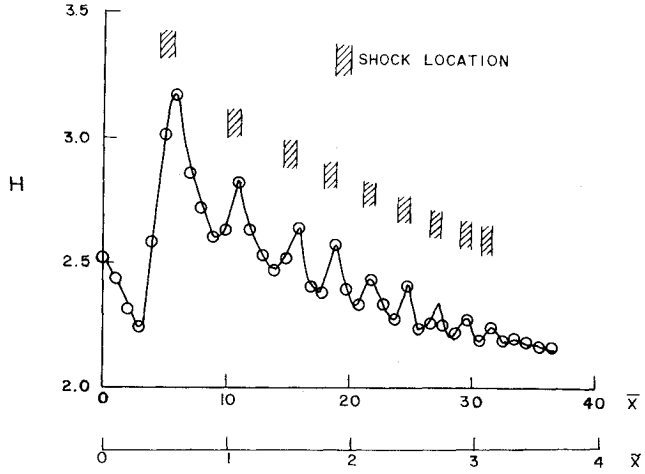

Fig. 11 Shape factor distribution.

and wall pressure into the momentum balance:

$$\frac{\rho_e u_e^2\left(\theta-\frac{\theta^2}{2R}\right)}{\left[\rho_e u_e^2\left(\theta-\frac{\theta^2}{2R}\right)\right]_u}-1=\int_{x_u}^{x}\frac{\left(\delta^*-\frac{\delta^{*2}}{2R}\right)\frac{dp}{dx}\,dx}{\left[\rho_e u_e^2\left(\theta-\frac{\theta^2}{2R}\right)\right]_u}$$

$$+\int_{x_u}^{x}\frac{C_f}{2}\frac{\rho_e u_e^2 dx}{\left[\rho_e u_e^2\left(\theta-\frac{\theta^2}{2R}\right)\right]_u}$$

The momentum thickness obtained from the above equation is compared with the experimental momentum thickness in Fig. 10. Considering the complexity of the flowfield, the comparison seems very satisfactory. This observation does not provide absolute proof of two-dimensionality, but suggests that the three-dimensional effects, if any, are very small.

Concluding Remarks

The results of the experimental investigation of the shock-wave/boundary-layer interaction at a freestream Mach number of 1.49, a unit Reynolds number of 4.90×10^6/m, and a blockage of 5.15% in a circular duct have led to the following conclusions.

The details of the flowfield show the formation of a series of normal shock waves with successively decreasing strength and decreasing distance between the successive shock waves up to the point where a terminal shock occurs. The presence of the multiple shock waves cannot be detected from the wall pressure distribution. On the other hand, the flowfield static pressure measurements clearly depict the multiple shock formation. The boundary-layer displacement thickness and shape factor distributions also show the presence of multiple shock waves. A one-dimensional flow model based on the boundary-layer displacement buildup may be used to explain the formation of the series of normal shock waves. A comparison with the results from our previous experiment involving a single shock interaction at nearly the same freestream Mach and Reynolds numbers, but at a lower blockage of 2.27%, indicates that the effect of increasing the blockage to 5.15% is to promote multiple shock interactions and produce a lower pressure recovery, a less retarded boundary-layer flow, and an increase in the overall length of the interaction.

Acknowledgments

This work was supported by NASA Grants NGR-48-002-047 and NGR-48-002-141 under the administration of the Aerodynamics Branch, Ames Research Center.

References

[1]Neumann, E. P. and Lustwerk, F., "Supersonic Diffusers for Wind Tunnels," *Journal of Applied Mechanics*, Vol. 16, June 1949, pp. 195-202.

[2]McLafferty, G. H., Krasnoff, E., Rannard, E., Rose, W. G., and Vergera, R., "Investigation of Turbojet Inlet Design Parameters," United Aircraft Corp., East Hartford, Conn., Rept. R-0790-13, Dec. 1955.

[3]Russell, D. A., "Gas Dynamics Lasers," *Astronautics & Aeronautics*, Vol. 13, No. 6, 1975, pp. 50-55.

[4]Kenny, D. P., "A Novel Low-Cost Diffuser for High Performance Centrifugal Compressors," *Journal of Engineering for Power*, Vol. 91, Jan. 1969, pp. 37-47.

[5]Lustwerk, F., "The Influence of Boundary Layer on the Normal Shock Configuration," Massachusetts Institute of Technology, Cambridge, Mass., Meteor Rept. 9661, Sept. 1950.

[6]Waltrup, P. J. and Billig, F. S., "Structure of Shock Waves in Cylindrical Ducts," *AIAA Journal*, Vol. 11, Oct. 1973, pp. 1404-1408.

[7]Merkli, P. E., "Pressure Recovery in Rectangular Constant Area Supersonic Diffusers," *AIAA Journal*, Vol. 14, Feb. 1976, pp. 168-172.

[8]Kamal, W. A. and Livesey, J. L., "Diffuser Inlet Flow Structure Following a Shock-Boundary Layer Interaction," *Fourth International Symposium on Air Breathing Engines*, Orlando, Fla., Paper No. 79-7026, April 1979, pp. 209-217.

[9]Waltrup, P. J. and Cameron, J. M., "Wall Shear and Boundary-Layer Measurements in Shock Separated Flow," *AIAA Journal*, Vol. 12, June 1974, pp. 878-880.

[10]Om, D., Viegas, J. R., and Childs, M. E., "Transonic Shock-Wave/Turbulent Boundary-Layer Interactions in a Circular Duct," *AIAA Journal*, Vol. 23, May 1985, pp. 707-714 (also AIAA Paper 82-0990, June 1982).

[11]Kooi, J. W., "Influence of Free-Stream Mach Number on Transonic Shock Wave Boundary Layer Interaction," Symposium on Transonic Configurations, NLR-MP-78013-U, Bad Harzburg, FRG, June 1978.

[12]Green, J. E., "Interactions Between Shock Waves and Turbulent Boundary Layers," *Progress in Aeronautical Science*, Vol. 11, 1970, pp. 235-340.

[13]Reda, C. D. and Murphy, J. D., "Shock Wave-Turbulent Boundary Layer Interactions in Rectangular Channels," AIAA Paper 72-715, 1972.

[14]Rose, W. C., "The Behavior of a Compressible Turbulent Boundary Layer in a Shock-Wave-Induced Adverse Pressure Gradient," NASA TN D-7092, March 1973.

[15]Om, D. and Childs, M. E., "An Experimental Investigation of Multiple Shock Wave/Turbulent Boundary Layer Interactions in a Circular Duct," AIAA Paper 82-1744, July 1983.

[16]Gray, J. D., "Evaluation of Probes for Measuring Static Pressure in Supersonic and Hypersonic Flows," AEDC-TR-71-265, Jan. 1972.

[17]Om, D., "A Study of Transonic Normal Shock Wave-Turbulent Boundary Layer Interactions in Axisymmetric Internal Flow," Ph.D. Thesis, University of Washington, Seattle, Wash., 1982.

[18]Reed, T. D., Pope, T. C., and Cooksey, J. M., "Calibration of Transonic and Supersonic Wind Tunnels," NASA CR 2920, Nov. 1977.

[19]Sun, C. C. and Childs, M. E., "A Modified Wall-Wake Velocity Profile for Turbulent Compressible Boundary Layers," *Journal of Aircraft*, Vol. 10, June 1973, pp. 381-383.

[20]Winter K. G. and Gaudet, L., "Turbulent Boundary-Layer Studies at High Reynolds Numbers at Mach Numbers Between 0.2 and 2.8," ARC R&M 3712, 1970.

[21]Seddon, J., "The Flow Produced by Interaction of a Turbulent Boundary Layer with a Normal Shock Wave of Strength Sufficient to Cause Separation," ARC R&M 3502, March 1960.

[22]Rubesin, M. W., Murphy, J. D., and Rose, W. C., "Wall Shear in Strongly Retarded and Separated Compressible Turbulent Boundary Layers," *AIAA Journal*, Vol. 12, Oct. 1974, pp. 1442-1444.